Oxidation-induced biquadratic coupling in Co/Fe/MgO/Fe(001)

Y. F. Chiang, Jared J. I. Wong, X. Tan, Yan Li, K. Pi, W. H. Wang, H. W. K. Tom, and R. K. Kawakami

Department of Physics and Astronomy, University of California, Riverside, California 92521, USA

We investigate the interlayer exchange coupling in Co/Fe/MgO/Fe(001) via molecular-beam epitaxy synthesis and magneto-optic Kerr effect measurements across wedged samples. By independently varying the oxygen contents of the MgO film and the Fe/MgO interface, the biquadratic coupling is found to be correlated with the interfacial oxidation. Furthermore, the temperature dependence indicates that the biquadratic coupling originates from indirect exchange interactions with magnetic impurities in the MgO spacer.

I. INTRODUCTION

The high values of room-temperature tunneling magnetoresistance (TMR) in Fe/MgO/Fe(001) and related MgO-based magnetic tunnel junctions (~400%) have attracted considerable interest from both the scientific and technological communities.[1–4] The theoretical prediction of TMR values exceeding several thousand percent in ideal structures provides motivation to further improve the synthesis and characterization of MgO-based heterostructures.[1,5] A central issue is the role of nonidealities such as interface oxidation, magnetic impurities, and oxygen vacancies in determining the magnetic and magnetotransport properties.[6–13] The interlayer exchange coupling (IEC) across MgO spacers is a fascinating phenomenon (both bilinear and biquadratic) and provides a means of investigating the relationship between the spin-dependent properties and the nonideal aspects of the system.[9,14–21]

In this paper, we show that the biquadratic coupling in Co/Fe/MgO/Fe(001) is correlated with the interfacial oxidation and originates from indirect exchange interactions with magnetic impurities in the MgO spacer (i.e., the loose spin model[18]). Using molecular-beam epitaxy (MBE) synthesis and magneto-optic Kerr effect (MOKE) measurements across wedged samples, we systematically investigate the role of interfacial oxidation on the IEC across MgO. First, we find that the biquadratic coupling strength increases with the oxygen pressure during MgO growth. To isolate the interface vs bulk effect, we systematically vary the oxidation of the lower Fe/MgO interface while maintaining the oxygen content of the MgO film. In this manner, the biquadratic coupling is found to be correlated with the interfacial oxidation. Furthermore, the temperature dependence of the biquadratic coupling exhibits a strong increase at low temperatures and the loose spin model is able to quantitatively account for this behavior.

II. EXPERIMENTAL PROCEDURES

Samples consisting of Ag(10 nm)/Co(50 nm)/Fe(5 nm)/MgO(wedge)/Fe(15 nm)/MgO(001) are grown on double-side-polished MgO(001) substrates. Following a 30 min anneal of the MgO substrate at 600 °C, the bottom Fe layer ("free layer") is grown at room temperature and subsequently annealed at 450 °C to generate an atomically flat surface.

The reflection high energy electron-diffraction (RHEED) pattern of the Fe film [Fig. 1(a)] has a weak 2×2 reconstruction which indicates the presence of carbon. In comparing samples with and without a MgO buffer layer to suppress carbon contamination, we find that there is no noticeable difference in the IEC, consistent with other studies.[22] Unless otherwise noted, the MgO layer is initiated by a 1 monolayer (ML) Mg template to reduce the oxidation of the bottom Fe interface.[23] Then oxygen gas (chamber pressure 2×10^{-8}–5×10^{-7} torr) is introduced into the ultrahigh vacuum chamber and elemental Mg is deposited at room temperature at a rate of ~0.06 nm/min to form MgO. The MgO growth rate is determined by measuring the deposition rate of elemental Mg by a quartz deposition monitor and multiplying by 0.80
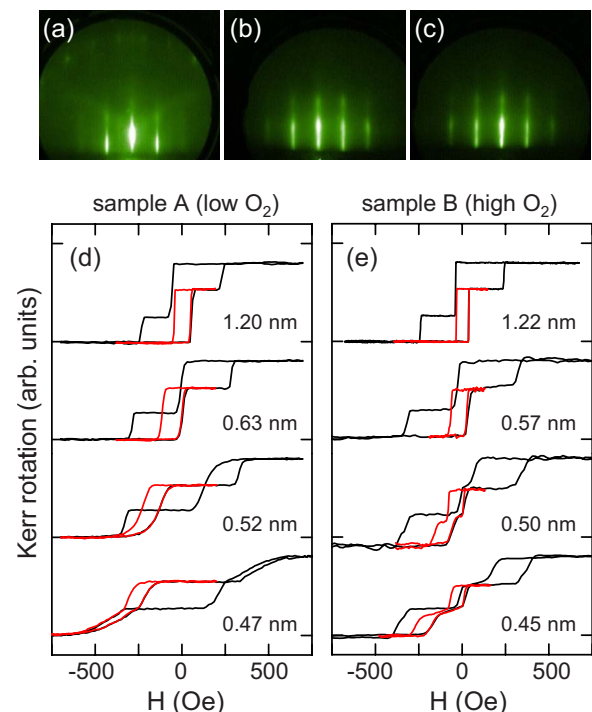

sample A (low O$_2$)   sample B (high O$_2$)

FIG. 1. (Color online) [(a)–(c)] RHEED patterns of the bottom Fe layer after annealing, MgO barrier layer grown at 2×10^{-8} torr, and MgO barrier layer grown at 2×10^{-7} torr, respectively. (d) Black curves are representative major hysteresis loops and red (dark gray) curves are corresponding minor hysteresis loops for sample A at various t_{MgO}. (e) Representative major (black) and minor (red or dark gray) hysteresis loops for sample B at various t_{MgO}.

to account for the higher density of Mg in MgO. This rate has been compared against RHEED oscillations on a calibration sample, and the rates agree to within 10%. Figures 1(b) and 1(c) show RHEED patterns for the MgO layers grown at chamber pressures of 2×10^{-8} and 2×10^{-7} torr, respectively. Auger-electron spectroscopy on these films exhibits O/Mg peak ratios of 4.1 and 5.5, respectively. The RHEED patterns indicate that the MgO lattice is capable of maintaining flat single-crystalline structure while incorporating different amounts oxygen deficiency. Finally, the Co/Fe bilayer ("hard layer") is deposited at room temperature and the entire structure is capped by Ag.

The effect of oxygen content on the IEC is investigated by comparing two wedged samples to MgO layers grown at different chamber pressures: 2×10^{-8} torr (sample A, "low O_2") and 5×10^{-7} torr (sample B, "high O_2"). The IEC is expressed as $E = -J_1 \cos(\theta_F - \theta_H) + J_2 \cos^2(\theta_F - \theta_H)$, where E is the energy per unit area, J_1 is the bilinear coupling coefficient, J_2 is the biquadratic coupling coefficient, and θ_F (θ_H) is the in-plane angle of the free (hard) layer magnetization. The magnetizations are in plane due to magnetic shape anisotropy. The values of J_1 and J_2 are obtained as a function of MgO thickness (t_{MgO}) by measuring hysteresis loops via longitudinal MOKE with magnetic field (H) along the [100] in-plane direction of Fe. Figures 1(d) and 1(e) show representative hysteresis loops for samples A and B at various t_{MgO}. For both samples, at large t_{MgO} the loops exhibit abrupt jumps at ~ 30 and ~ 250 Oe, which correspond to the independent magnetization reversals of the free layer (bottom Fe) and hard layer (Co/Fe bilayer), respectively. The much higher coercivity of the hard layer enables the determination of both J_1 and J_2 (within the macrospin approximation[24]) by measuring minor hysteresis loops (red or dark gray curves) in which the hard layer is not switched. The minor loops start at negative saturation so that the hard layer is always oriented along the negative direction ($\theta_H = 180°$), and the energy per unit area of the free layer is therefore given by

$$E(\theta_F, H) = -(HM_F t_F - J_1)\cos\theta_F + J_2 \cos^2\theta_F$$
$$+ K_F t_F \cos^2(\theta_F)\sin^2(\theta_F), \qquad (1)$$

where M_F is the magnetization, t_F is the thickness, and K_F is the cubic anisotropy of the free layer. The anisotropy, K_F, is determined by measuring the saturation field of a 15 nm Fe/MgO(001) sample with the field applied along the in-plane hard axis of the Fe (i.e., the [110] axis). At room temperature, K_F is 5.0×10^5 erg/cm^3 and increases to 6.9×10^5 erg/cm^3 at 5 K. Figure 2(a) illustrates the shifting (H_1) and splitting ($2H_2$) of the minor loop for sample B at $t_{MgO} = 0.45$ nm. The shifting and splitting of the minor loop yield values for J_1 and J_2 based on the energy minimization of Eq. (1). Through a change of variables to $h = H - H_1$, with $H_1 \equiv J_1/M_F t_F$, the energy reduces to

$$E(\theta_F, h) = -hM_F t_F \cos(\theta_F) + J_2 \cos^2(\theta_F)$$
$$+ K_F t_F \cos^2(\theta_F)\sin^2(\theta_F), \qquad (2)$$

which implies that J_1 shifts the minor loop to be centered at $H = H_1$. In Fig. 2(a), the negative value of H_1 indicates antiferromagnetic (AF) coupling ($J_1 < 0$).
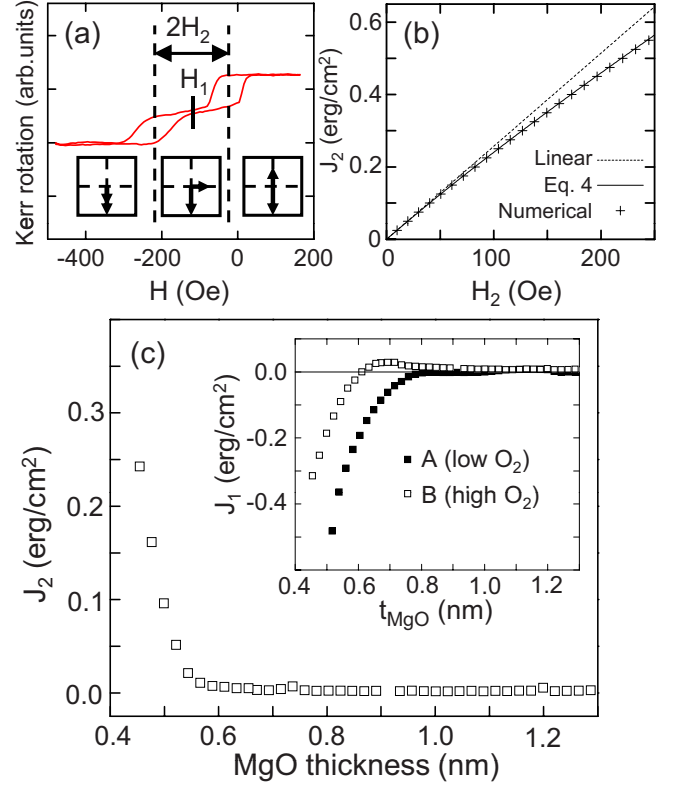

FIG. 2. (Color online) (a) Illustration of the shifting (H_1) and splitting ($2H_2$) of a minor hysteresis loop. The pictured loop is from sample B at $t_{MgO} = 0.45$ nm. (b) J_2 as a function of H_2 comparing Eq. (4) to numerical minimization of Eq. (2) and with $J_2 \approx H_2 M_F t_F$. We assume $M_F = 1714$ emu/cm^3 for Fe. (c) Biquadratic coupling coefficient J_2 as a function of t_{MgO} for sample B. Inset: Bilinear coupling coefficient J_1 as a function of t_{MgO} for samples A and B.

For biquadratic coupling ($J_2 > 0$), the minor loop splits due to 90° magnetization switchings of the free layer that occur when the global energy minimum changes from a saturated state ($\theta_F = 0°$ or $180°$) to an intermediate state ($\theta_F \sim 90°$) or vice versa. For positive h, one local minimum is at positive saturation: $E_{sat} = -hM_F t_F + J_2$. Another local minimum is for the intermediate state near 90°, where we define a small angle δ by $\theta_F = 90° + \delta$ to yield $E_{int} = hM_F t_F \delta + J_2 \delta^2 + K_F t_F \delta^2 + O(\delta^3)$. The condition for $|\delta| \ll 1$ is equivalent to $J_2 \ll K_F t_F$. Keeping up to second order in δ, the value of E_{int} is minimized by setting $dE_{int}/d\delta = 0$ and the corresponding energy is given by $E_{int} \approx -(hM_F t_F)^2/4(J_2 + K_F t_F)$. The switching field H_2 is defined as the value of h where the global energy minimum switches between E_{sat} and E_{int}. Thus, H_2 is given by $E_{sat} = E_{int}$ or $-H_2 M_F t_F + J_2 \approx -(H_2 M_F t_F)^2/4(J_2 + K_F t_F)$. Solving for H_2 yields

$$H_2 \approx 2[J_2 + K_F t_F - \sqrt{K_F t_F (J_2 + K_F t_F)}]/M_F t_F. \qquad (3)$$

A similar expression for H_2 is obtained for the case of negative h, except that there is an overall negative sign. Therefore, the total splitting of the minor loop is given by $2H_2$. Solving for J_2 yields the useful expression

$$J_2 \approx \frac{1}{2}\left(-K_F t_F + H_2 M_F t_F + \sqrt{K_F t_F (K_F t_F + 2H_2 M_F t_F)}\right).$$

$$(4)$$

In the limit of $J_2 \ll K_F t_F$, this reduces to the simple relation $J_2 \approx H_2 M_F t_F$. This simple relation can also be obtained by following the procedure above, but setting $\delta = 0$. Figure 2(b) compares the linear relation $J_2 \approx H_2 M_F t_F$ (dashed line) and Eq. (4) (solid line) with the exact solution (crosses) obtained by numerical minimization of Eq. (2). We find that Eq. (4) is very accurate, while the linear relation is valid for lower values of H_2 (for $H_2 < 100$ Oe, the error is less than 10%). The improved accuracy of Eq. (4) compared to the simple relation $J_2 \approx H_2 M_F t_F$ is because the former keeps terms of up order δ^2 in the calculation while the latter assumes $\delta = 0$.

Apart from the biquadratic coupling, we verify that the split loop does not originate from in-plane uniaxial magnetic anisotropy by measuring minor loops with the sample rotated in plane by 90° and minor loops with equivalent splittings are observed; a uniaxial anisotropy would exhibit split loops only along one of these axes.[25] Another possible explanation of the split loop is the stabilization of the 90° alignment by a combination of four-fold anisotropy and AF coupling,[26] which occurs in models that go beyond the macrospin approximation.[27,28] Subsequent data will show that this effect does not contribute significantly to our results.

III. RESULTS AND DISCUSSION

Looking at the representative minor loop for sample A at $t_{MgO} = 1.20$ nm [Fig. 1(d)], a square minor loop centered at the origin indicates the absence of J_1 and J_2 (below measurement sensitivity of ~0.005 erg/cm^2). With decreasing t_{MgO}, the minor loop shifts toward the negative field direction which corresponds to an increasing AF coupling strength. Interestingly, the minor loop does not split into two subloops at any t_{MgO} so that biquadratic coupling is not observed in this sample. At $t_{MgO} = 0.47$ nm, the AF coupling is so strong that the hard layer no longer remains at $\theta_H = 180°$ during the minor loop sweep so that Eq. (1) is no longer valid and J_1 and J_2 are not easily determined. Turning to sample B [Fig. 1(e)], at $t_{MgO} = 1.22$ nm a square minor loop centered at the origin indicates the absence of interlayer coupling within the measurement sensitivity. At $t_{MgO} = 0.57$ nm, the minor loop is centered on a negative field direction which indicates AF coupling. At $t_{MgO} = 0.50$ nm, the minor loop begins to split which indicates the presence of biquadratic coupling ($J_2 > 0$), and at 0.45 nm the magnitudes of J_1 and J_2 have increased further.

The detailed dependence of J_1 and J_2 on t_{MgO} is obtained by scanning the MOKE measurement along the MgO wedge [Fig. 2(c)]. On sample A, biquadratic coupling is not observed for any t_{MgO}. On sample B (open squares), the biquadratic coupling has a value of 0.24 erg/cm^2 at 0.45 nm, decreases monotonically with increasing t_{MgO}, and becomes undetectable beyond $t_{MgO} \sim 0.6$ nm. The presence of J_2 in sample B and the absence of J_2 in sample A imply that the oxygen content is an important factor for generating the biquadratic coupling. In terms of J_1, both samples exhibit AF
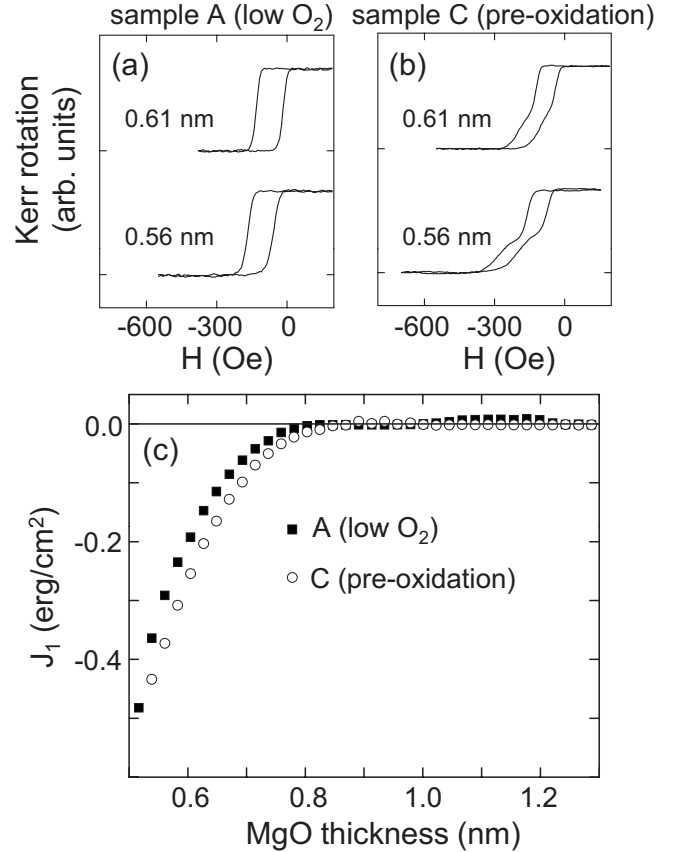

FIG. 3. (a) Minor hysteresis loops from sample A at various t_{MgO}. (b) Minor hysteresis loops from sample C at corresponding t_{MgO}. (c) A comparison of bilinear coupling for samples A and C as a function of t_{MgO}.

coupling whose strength decays with increasing t_{MgO} [inset of Fig. 2(c)] and sample B experiences a crossover to weak ferromagnetic coupling at $t_{MgO} = 0.60$ nm. This behavior is consistent with previous experimental and theoretical studies.[9,14,15] The stronger AF coupling in sample A may either be due to having more oxygen vacancies (cf. impurity state model[9]) or a decrease in the barrier height (cf. spin-dependent tunneling model[14,16,17]), but further studies are needed to determine the physical origin of J_1.

To gain insight into the origin of the biquadratic coupling, we systematically vary the bottom Fe/MgO interface to separate the interface vs bulk effect with regards to the role of oxygen content. In a first approach, we grow a sample that combines a higher level of Fe/MgO interface oxidation with low oxygen content for the MgO film (sample C, "pre-oxidation"). This is accomplished by exposing the sample to 2×10^{-6} torr oxygen pressure for ~2 min after the 1 ML Mg template is deposited. Then the oxygen pressure is reduced to 2×10^{-8} torr and the Mg is deposited to form an MgO film with oxygen content similar to sample A. Figures 3(a) and 3(b) show representative minor loops from samples A and C, respectively, for various t_{MgO}. While the minor loops from sample A do not exhibit any splittings, the minor loops from sample C show noticeable splittings at corresponding thicknesses. Although the split loops are not perfectly symmetric, they clearly indicate biquadratic coupling.
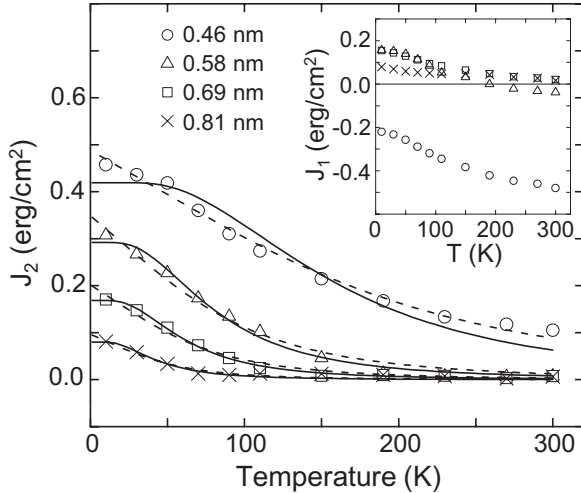
FIG. 4. Temperature dependence of biquadratic coupling on a step-wedge sample at t_{MgO}=0.46, 0.58, 0.69, and 0.81 nm. Solid lines are curve fits based on the loose spin model with loose spins located at the interfaces (U_1 and U_2 are fitting parameters and c=2). Dashed lines are curve fits based on the loose spin model with loose spins uniformly distributed throughout the spacer (c and U_1=U_2 are fitting parameters). Inset: Temperature dependence of bilinear coupling for t_{MgO}=0.46, 0.58, 0.69, and 0.81 nm.

This provides strong evidence that the biquadratic coupling is correlated with interfacial oxidation (which is present to some degree in all Fe/MgO interfaces[6]). In comparing the bilinear coupling in samples A and C [Fig. 2(c)], the values of J_1 are very similar for the two samples. These data argue against pinholes as the origin of J_2 (Ref. 14) because pinholes should promote ferromagnetic coupling in J_1, but the enhancement of J_2 in sample C is not accompanied by a shift in J_1 toward ferromagnetic coupling. Data also argue against the major contribution to the split loops originating from four-fold anisotropy+AF coupling because the increase in the splitting of the loops should be accompanied by an increase in the AF coupling,[27,28] but this is not observed.

To investigate the origin of the biquadratic coupling, we measure the temperature dependence of IEC on a MgO step-wedge sample with the MgO grown at 4×10^{-7} torr (sample D). Figure 4 shows the temperature dependences of J_1 and J_2 for t_{MgO}=0.46, 0.58, 0.69, and 0.81 nm. J_2 is calculated from Eq. (4) with K_F values measured as a function of temperature. J_2 increases dramatically at low temperatures, while J_1 shifts toward ferromagnetic coupling. This behavior (including a sign change in J_1 for t_{MgO}=0.58 nm) is not explained by existing models of the bilinear coupling,[9,16,17] so further study is necessary. We note that this behavior is also present on samples where the MgO layer is grown by *e*-beam deposition and samples employing a MgO buffer layer to suppress carbon contamination. This behavior argues against any major contribution from the four-fold anisotropy+AF effect because the splitting of the loops increases while the AF coupling decreases, which is opposite of the predicted behavior for this mechanism.[27,28] In addition, substantial

splitting is observed at low temperatures even in the absence of AF coupling. Therefore, it is clear that the observed changes in the splitting are due to the biquadratic coupling. The strong temperature dependence of J_2 is consistent with biquadratic coupling mediated by magnetic impurities in the spacer (loose spin model).[18] Because J_2 is correlated with interfacial oxidation, we first perform the fitting for interfacial loose spins (c=2, $U_1 \neq U_2$), where c is the fractional concentration of loose spins and U_1 and U_2 are the exchange couplings between a loose spin and the ferromagnetic layers.[18] The solid lines in Fig. 4 are the best fits with values of $|U_1|/k_B$=27.4, 16.5, 10.9, and 6.34 K and $|U_2|/k_B$=299.3, 155.1, 117.6, and 83.8 for t_{MgO}=0.46, 0.58, 0.69, and 0.81 nm, respectively. In another approach, if the loose spins are uniformly distributed throughout the spacer, then one assumes that U_1=U_2 and c is treated as a fitting parameter.[18] The dashed curves are the best fit with values of $|U_1|/k_B$=$|U_2|/k_B$=344.8, 166.2, 125.1, and 89.8 K and c=0.025, 0.03, 0.023, and 0.016 for t_{MgO}=0.46, 0.58, 0.69, and 0.81 nm, respectively. Both fitting approaches are able to account for the strong temperature dependence, but neither approach is clearly better. Data exhibit hints of plateaus at the lowest temperatures, which is a characteristic of interfacial loose spins and the first approach produces somewhat better fits for t_{MgO}=0.58 and 0.69 nm. On the other hand, the second approach has a better fit for t_{MgO}=0.46 nm. A possible scenario is that the magnetic impurities segregate away from the interface during MgO growth. Most importantly, regardless of the exact spatial distribution of the loose spins, this model is able to quantitatively account for the strong temperature dependence of J_2. On the other hand, other possible sources of biquadratic coupling such as the interfacial step mechanism[19] and the magnetic-dipole mechanism[29] cannot explain the temperature dependence even qualitatively. Thus, the experimental evidence strongly supports the loose spin mechanism as the origin of the biquadratic coupling across MgO.

In summary, by varying the oxygen pressure during the MgO growth and using minor hysteresis loop analysis, we demonstrate that the IEC depends on the oxygen content within the Co/Fe/MgO/Fe system. Samples with MgO grown at low oxygen pressure exhibit only bilinear coupling, while samples with MgO grown at high oxygen pressure exhibit both bilinear and biquadratic coupling. Further investigation reveals that the presence of biquadratic coupling is due to the oxidation of the lower MgO/Fe interface. Finally, the strong temperature dependence of the biquadratic coupling and quantitative analysis of the data provides strong evidence for the loose spin mechanism as the source of the biquadratic coupling.

[1] W. H. Butler, X. G. Zhang, T. C. Schulthess, and J. M. MacLaren, Phys. Rev. B **63**, 054416 (2001).

[2] S. S. P. Parkin, C. Kaiser, A. Panchula, P. M. Rice, B. Hughes, M. Samant, and S.-H. Yang, Nature Mater. **3**, 862 (2004).

[3] S. Yuasa, T. Nagahama, A. Fukushima, Y. Suzuki, and K. Ando, Nature Mater. **3**, 868 (2004).

[4] S. Yuasa, A. Fukushima, H. Kubota, Y. Suzuki, and K. Ando, Appl. Phys. Lett. **89**, 042505 (2006).

[5] X.-G. Zhang and W. H. Butler, Phys. Rev. B **70**, 172407 (2004).

[6] H. L. Meyerheim, R. Popescu, N. Jedrecy, M. Vedpathak, M. Sauvage-Simkin, R. Pinchaux, B. Heinrich, and J. Kirschner, Phys. Rev. B **65**, 144433 (2002).

[7] X.-G. Zhang, W. H. Butler, and A. Bandyopadhyay, Phys. Rev. B **68**, 092402 (2003).

[8] C. Tusche, H. L. Meyerheim, N. Jedrecy, G. Renaud, A. Ernst, J. Henk, P. Bruno, and J. Kirschner, Phys. Rev. Lett. **95**, 176101 (2005).

[9] M. Y. Zhuravlev, E. Y. Tsymbal, and A. V. Vedyayev, Phys. Rev. Lett. **94**, 026806 (2005).

[10] B. D. Yu and J.-S. Kim, Phys. Rev. B **73**, 125408 (2006).

[11] P. G. Mather, J. C. Read, and R. A. Buhrman, Phys. Rev. B **73**, 205412 (2006).

[12] J. P. Velev, K. D. Belashchenko, S. S. Jaswal, and E. Y. Tsymbal, Appl. Phys. Lett. **90**, 072502 (2007).

[13] C. Tusche, H. L. Meyerheim, N. Jedrecy, G. Renaud, and J. Kirschner, Phys. Rev. B **74**, 195422 (2006).

[14] J. Faure-Vincent, C. Tiusan, C. Bellouard, E. Popova, M. Hehn, F. Montaigne, and A. Schuhl, Phys. Rev. Lett. **89**, 107206 (2002).

[15] T. Katayama, S. Yuasa, J. Velev, M. Y. Zhuravlev, S. S. Jaswal, and E. Y. Tsymbal, Appl. Phys. Lett. **89**, 112503 (2006).

[16] J. C. Slonczewski, Phys. Rev. B **39**, 6995 (1989).

[17] P. Bruno, Phys. Rev. B **49**, 13231 (1994).

[18] J. C. Slonczewski, J. Appl. Phys. **73**, 5957 (1993).

[19] J. C. Slonczewski, Phys. Rev. Lett. **67**, 3172 (1991).

[20] E. Snoeck, P. Baules, G. BenAssayag, C. Tiusan, F. Greullet, M. Hehn, and A. Schuhl, J. Phys.: Condens. Matter **20**, 055219 (2008).

[21] B. Heinrich, Z. Celinski, J. F. Cochran, A. S. Arrott, K. Myrtle, and S. T. Purcell, Phys. Rev. B **47**, 5077 (1993).

[22] C. Tiusan, M. Sicot, J. Faure-Vincent, M. Hehn, C. Bellouard, F. Montaigne, S. Andrieu, and A. Schuhl, J. Phys.: Condens. Matter **18**, 941 (2006).

[23] Y. Lu, C. Deranlot, A. Vaures, F. Petroff, J. M. George, Y. Zheng, and D. Demailles, Appl. Phys. Lett. **91**, 222504 (2007).

[24] S. O. Demokritov, J. Phys. D **31**, 925 (1998).

[25] W. Weber, C. H. Back, A. Bischof, C. Würsch, and R. Allenspach, Phys. Rev. Lett. **76**, 1940 (1996).

[26] C. Bellouard, J. Faure-Vincent, C. Tiusan, F. Montaigne, M. Hehn, V. Leiner, H. Fritzsche, and M. Gierlings, Phys. Rev. B **78**, 134429 (2008).

[27] W. Folkerts and S. T. Purcell, J. Magn. Magn. Mater. **111**, 306 (1992).

[28] J. F. Cochran, J. Magn. Magn. Mater. **147**, 101 (1995).

[29] S. Demokritov, E. Tsymbal, P. Grunberg, W. Zinn, and I. K. Schuller, Phys. Rev. B **49**, 720 (1994).